Optical anisotropy in the electronic nematic phase of FeSe

M. Chinotti, A. Pal, L. Degiorgi, A. E. Böhmer, and P. C. Canfield

Phys. Rev. B **96**, 121112 — Published 18 September 2017

DOI: 10.1103/PhysRevB.96.121112

Optical Anisotropy in the Electronic Nematic Phase of FeSe

M. Chinotti, A. Pal, and L. Degiorgi*
Laboratorium für Festkörperphysik, ETH - Zürich, 8093 Zürich, Switzerland

A.E. Böhmer and P.C. Canfield
Ames Laboratory, Ames, Iowa 50010, USA

At ambient pressure FeSe undergoes a structural, tetragonal-to-orthorhombic, phase transition at $T_s \simeq 90$ K without any magnetic ordering on further cooling. FeSe thus provides an arena for examining the nematic phase without the complications following the reconstruction of the Fermi surface due to the antiferromagnetic order within the orthorhombic state. We perform an optical-reflectivity investigation across the structural transition, as a function of uniaxial stress in order to detwin the specimen. These measurements reveal a hysteretic behavior of the anisotropic optical response to uniaxial stress for $T \leq T_s$, which extends to energy scales of about 0.5 eV. The sign changes of the optical anisotropy between distinct energy intervals suggest a complex evolution of the polarized electronic structure in the nematic phase. The temperature dependence of the optical anisotropy for the fully detwinned specimen is furthermore acting as a proxy for the order parameter of nematicity.

PACS numbers: 64.70.M-,74.70.Xa,78.20.-e

Superconductivity at high temperature often develops in proximity to symmetry-breaking states. The nematic state, in which the electron system breaks a discrete rotational symmetry of the crystal lattice without altering the existing translational symmetry, has emerged as a key concept in iron-based superconductors and may be intimately related to the pairing mechanism of superconductivity itself[1]. Nematicity was originally invoked in order to account for the anisotropy in the *dc* transport properties of the archetypal Co-underdoped 122-materials $Ba(Fe_{1-x}Co_x)_2As_2$ below the structural tetragonal-to-orthorhombic phase transition at T_s[2,3], which is larger than expected from the tiny orthorhombic lattice distortion alone.

Recently, we studied the optical reflectivity[4,5] as a function of temperature (T) across the structural phase transition for underdoped compositions of $Ba(Fe_{1-x}Co_x)_2As_2$, with uniaxial and $in-situ$ tunable applied stress which acts as a conjugate field to the orthorhombic distortion and circumvents sample twinning below T_s[6]. Above T_s, this stress induces a finite value of the orthorhombic distortion[2]. At temperatures $T < T_s$, the optical anisotropy exhibits a remarkable hysteretic response to the applied stress even at energies deep into the electronic structure. The anisotropy turns into a reversible linear stress dependence at $T \geq T_s$. Our results indicate an important polarization of the electronic structure in the nematic phase below T_s and a significant stress-induced one above T_s, related to the substantial nematic susceptibility[7].

In $Ba(Fe_{1-x}Co_x)_2As_2$, as in most Fe arsenide and chalcogenide superconductors, the structural phase transition either accompanies or precedes the onset of long range magnetic order and therefore the nematic and magnetic states are likely intertwined with each other. Consequently, the effects of the Fermi surface folding and thus of its reconstruction because of the antiferromagnetic order make it difficult to unambiguously address the intrinsic properties of the nematic state over a large temperature range. In this context, FeSe is very well suited in order to shed light on nematicity, since it harbors a tetragonal-to-orthorhombic structural phase transition at $T_s \simeq 90$ K, where the lattice breaks the $C4$ rotational symmetry, in the absence of any subsequent, ambient pressure long-range magnetic order. FeSe is then superconducting below $T_c = 8$ K[8,9].

Here, we describe results of reflectivity ($R(\omega)$) measurements on FeSe that probe the optical response to variable uniaxial stress at temperatures below and above T_s, in the energy interval from the infrared up to the visible spectral range. Our measurements at $T < T_s$ reveal a strong polarization dependence of the reflectivity spectra with respect to the orthorhombic axes and clearly demonstrate that the electronic anisotropy associated with the orthorhombicity extends far from the Fermi energy and also persists in the superconducting state. While the observed hysteretic behavior of the stress-dependent optical anisotropy in FeSe at $T \leq T_s$ shares some qualitative similarities with our earlier findings in the electron doped 122-materials, it yet displays an even more complex behavior than in $Ba(Fe_{1-x}Co_x)_2As_2$[4,5], with two sign changes on increasing frequency (i.e., the polarization dependence of $R(\omega)$ is opposite in distinct energy intervals). Moreover, we discover that the stress-induced orthorhombic distortion above T_s may couple differently to the complex orbital order occurring in FeSe than in $Ba(Fe_{1-x}Co_x)_2As_2$. This reveals important peculiarities of the two classes of materials in the response of their electronic structure to nematicity. Our results favor models for the nematic phase, which have to go beyond a simple ferro-orbital order scenario, as recently envisaged by ARPES data[10–13].

Large single crystals of FeSe were grown using chemical vapor transport, similarly to the description in Ref. 14.

The samples were mounted into our home-made device for applying stress and placed inside a Janis cryostat coupled to a Bruker Vertex 80v, Fourier-transform infrared interferometer. The device, described in detail in Refs. 4 and 5, consists of a spring bellows, which can be extended/retracted by flushing He-gas into its volume or evacuating it, thus exerting and releasing uniaxial stress on the lateral side of the specimen. The specimens of 0.3 mm thickness and approximate in-plane dimensions of 2x1.2mm^2 were cut and oriented such that the uniaxial stress (p), detwinning the samples, is applied parallel to the short orthorhombic axis, which at $T < T_s$ is preferentially aligned along the direction of a compressive stress (lower left panel of Fig. 1). As in Refs. 4 and 5, we refer here to the He-gas pressure inside the volume of the bellows ($p_{bellows}$): the effective stress felt by the sample (p_{sample}) depends on its size and thickness, so that $p_{bellows} = 0.1$ bar corresponds to an effective uniaxial stress of about $p_{sample} \sim 1.5$ MPa on our FeSe crystals. It has been widely established that an effective stress of at least 10 MPa is enough to fully detwin the specimen and thus reveal the underlying symmetry-breaking[2]. $R(\omega)$ as a function of T and $in-situ$ tunable p was measured at nearly normal incidence[15] with the electromagnetic radiation polarized along the orthorhombic elongated a ($R_a(\omega)$) and short b ($R_b(\omega)$) axes in a broad spectral range from the far-infrared up to the ultra-violet. Our results were obtained from zero-pressure-cooled (ZPC) 'pressure-loop' (at fixed T) and pressure-cooled (PC) 'fixed-pressure' (as a function of T) experiments[4,5]. Further details about this experiment can be found in the Supplemental Material (SM)[16].

Representative $R(\omega)$ data of FeSe in the infrared and mid-infrared (MIR) spectral range (i.e., for $500 \leq \omega < 6000$ cm^{-1}) are shown in the main panel of Fig. 1(a) at 10 K and with $p_{bellows} = 1.2$ bar following an initial ZPC protocol. Even though we mainly focus our attention in the MIR interval, it is worth emphasizing the overall metallic optical response of FeSe, shown in the inset of Fig. 1(a). The anisotropy of $R(\omega)$ between the two polarization directions is clearly visible in the raw data. A first general observation is that the optical polarization dependence vanishes at photon frequencies above 6000 cm^{-1} (0.74 eV), which is true for all temperatures. At $T < T_s$, we identify two distinct spectral ranges centered around 1000 and 3000 cm^{-1} (0.12 and 0.37 eV, respectively), where the optical anisotropy peaks upon increasing stress, yet with opposite sign (i.e., $R_a(\omega) > R_b(\omega)$ and $R_a(\omega) < R_b(\omega)$ around 1000 and 3000 cm^{-1}, respectively). Furthermore, even though not shown explicitly, $R_a(\omega) < R_b(\omega)$ at $T < T_s$ when entering the far infrared spectral range toward the dc limit (i.e., $\omega < 500$ cm^{-1} (62 meV)), thus reversing again the sign of the optical anisotropy.

In order to emphasize the evolution of the optical anisotropy as a function of p and T, we calculate the quantity $\Delta R_{ratio}(\omega) = (R_a(\omega)/R_b(\omega))$ - 1, representing the deviation from isotropic behavior, so that $\Delta R_{ratio}(\omega) > 0$ and $\Delta R_{ratio}(\omega) < 0$ at 1000 and 3000 cm^{-1}, respectively. Panels (b-g) of Fig. 1 show the p-dependence of $\Delta R_{ratio}(\omega)$ at 10, 60 and 100 K obtained from ZPC p-loop experiments. At 10 K (i.e., $T << T_s$) $|\Delta R_{ratio}(\omega)|$ in both ranges of interest (i.e., above/below 1500 cm^{-1}) is progressively enhanced and tends to saturate when p is increased. At this temperature, the anisotropy is almost completely retained when stress is subsequently released back to 0. At $T << T_s$, there is a weak polarization dependence of $R(\omega)$ even at zero applied p (Fig. 1(b)), likely due to some degree of detwinning because of the differential thermal contraction between the sample and the p-device itself[16]. At higher temperatures the overall enhancement of $|\Delta R_{ratio}(\omega)|$ upon applying p is smaller than that at 10 K in both ranges, and drops to a smaller value when p is released. At 100 K (i.e., $T > T_s$), the p-dependence of $|\Delta R_{ratio}(\omega)|$ is vanishingly small and the anisotropy is quite completely suppressed around 3000 cm^{-1} upon sweeping p, within our experimental error. Nonetheless, close and just above T_s $\Delta R_{ratio}(\omega)$ tends to get slightly negative at frequencies around 1000 cm^{-1}, which implies $R_b(\omega) > R_a(\omega)$ (Fig. 1(f-g)) already at infrared frequencies. This weak optical anisotropy persists even upon applying p and extends to the infrared range.

We first focus our attention on the p-dependence of ΔR_{ratio} at 1000 and 3000 cm^{-1} (dashed vertical lines in Fig. 1) for the ZPC p-loop measurements, shown in Fig. 2 for several representative temperatures[17]. For temperatures $T < T_s$ we encounter a clear half-hysteresis with opposite sign in the p-dependence of ΔR_{ratio}, which is likely due to twin boundary motion. The virgin curve shows a quite rapid enhancement in $|\Delta R_{ratio}|$ at low T, before the optical anisotropy starts to saturate for larger p (Fig. 2(a-b) and (f-g)). Therefore, we establish that a relatively modest uniaxial stress of $p_{sample} \sim 6$ MPa is able to detwin the sample in the orthorhombic phase. The saturation of ΔR_{ratio} at $T << T_s$ presumably reflects complete detwinning of the sample, and any subsequent p-dependence arises from the intrinsic response to p of the orthorhombic structure. For temperatures $T \leq T_s$ the initial curve increases smoothly and the saturation in the optical anisotropy is achieved more gradually (Fig. 2(c) and (h)). At T_s (Fig. 2(d) and (i)), the half-hysteresis loop has essentially collapsed and for $T \geq T_s$ (Fig. 2(e) and (j)) the material is tetragonal and no half-hysteresis is observed so that the optical anisotropy totally vanishes at 3000 cm^{-1} and is weakly negative at 1000 cm^{-1}.

By releasing p back to 0 the remanent optical anisotropy, due to the imbalance of the two twin orientations that remain frozen in place, can be probed[4]. At 10 K, the material barely shows changes in the optical anisotropy when p is released, indicating that the sample remains in a near-single domain state. In this case, ΔR_{ratio} at released $p = 0$ directly yields the intrinsic optical anisotropy of a fully detwinned but stress-free material. For increasing T, the anisotropy at released $p = 0$ gets suppressed as expected due to the thermally

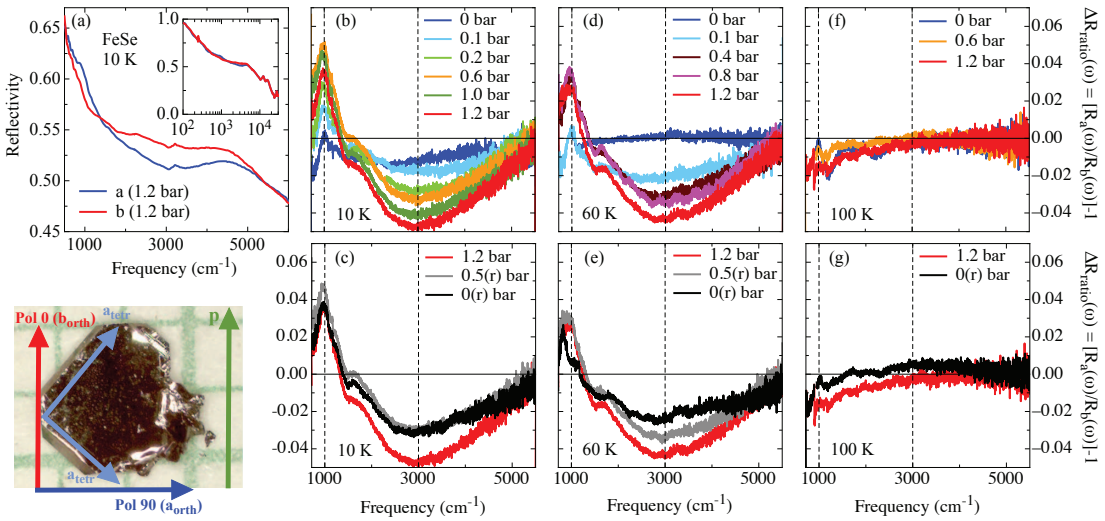

FIG. 1: (color online) Representative data of the optical reflectivity ($R(\omega)$) of FeSe for ZPC experiments: (a) $R(\omega)$ measured at 10 K with applied uniaxial stress of $p_{bellows} = 1.2$ bar (i.e., $p_{sample} = 18.5$ MPa felt by the sample) along the orthorhombic a ($R_a(\omega)$) and b ($R_b(\omega)$) axes, displaying the optical anisotropy in the infrared and mid-infrared spectral range. The inset shows $R_a(\omega)$ and $R_b(\omega)$ from the far-infrared up to the ultraviolet range with a logarithmic frequency scale. (b-g) p-dependence of $\Delta R_{ratio}(\omega)$ (see text) at 10, 60 and 100 K for increasing (b,d,f) and decreasing (c,e,g) p. Released p is noted by (r). The lower left panel shows a typical FeSe sample and emphasizes its orientation with respect to the directions of the applied stress p and polarization (Pol) of light[16].

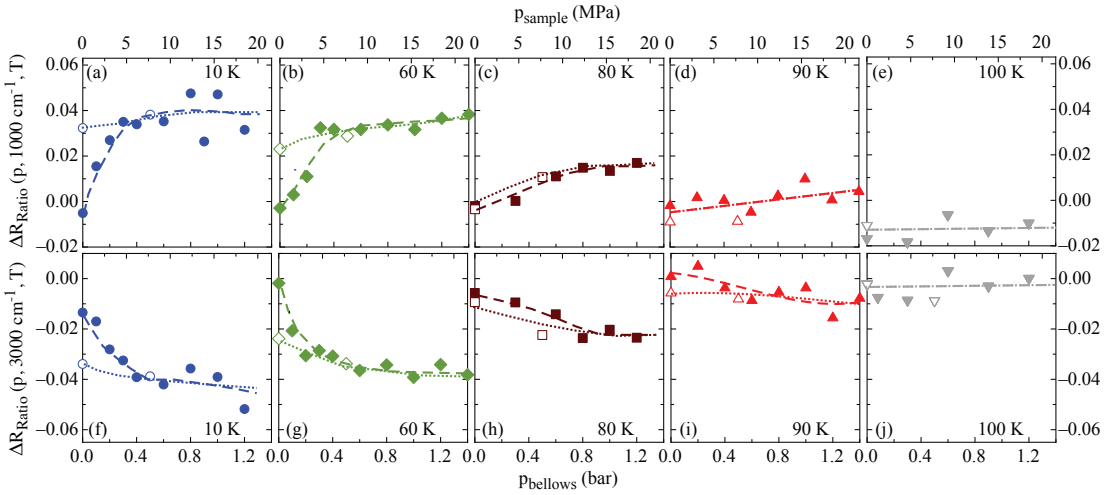

FIG. 2: (color online) (a-j) Optical anisotropy ΔR_{ratio} read at 1000 and 3000 cm^{-1} (dashed vertical lines in Fig. 1(b-g)) of FeSe as a function of applied stress p at representative temperatures[17]: full and open symbols denote increasing and decreasing p, respectively, for p-loop measurements following an initial ZPC protocol. Lower x-axis denotes He-gas p in the spring bellows ($p_{bellows}$) and upper x-axis the effective stress felt by the sample (p_{sample}). Dashed (increasing p) and dotted lines (releasing p) are drawn to guide the eye.

assisted domain-wall motion[4].

Before going any further, we mention the results of the PC measurements (for details and data see Ref. 16). Cooling the specimen across T_s at fixed, effectively felt stress of about 15 MPa leads to $\Delta R_{ratio}(T)$ that closely coincides with the anisotropy at saturation in the half-hysteresis p-loops. Therefore, the same optical anisotropy is obtained whether p_{sample} is increased above 10 MPa following a ZPC p-loop experiment or the sample is cooled through T_s at such constant p.

Figure 3 summarizes the T-dependence of ΔR_{ratio} for FeSe at 1000 and 3000 cm^{-1} read at fixed $p_{bellows} = 1.2$ bar (i.e., at saturation (sat), ΔR^{sat}_{ratio}) from the p-loop experiment within the ZPC procedure (Fig. 2), normalized by this quantity at 5 K. ΔR^{sat}_{ratio} at both energy scales undergoes a quite sharp onset at T_s and tends to flatten out below $T_s/2$. We reiterate that at 1000 cm^{-1} $\Delta R^{sat}_{ratio} < 0$ slightly above T_s, anticipating an incipient

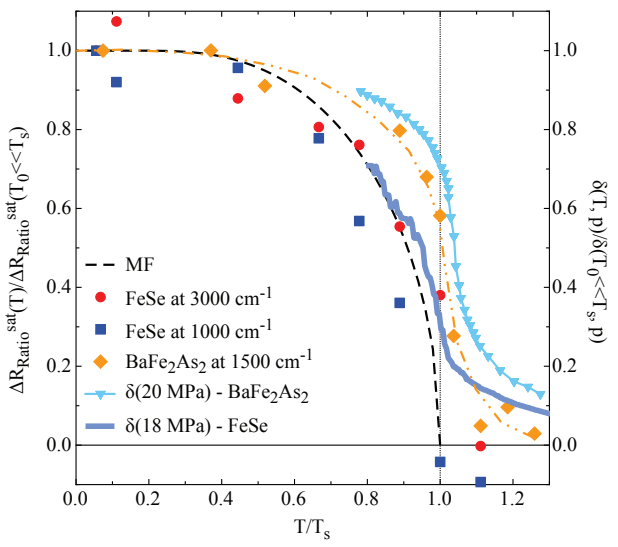

FIG. 3: (color online) Temperature dependence of ΔR^{sat}_{ratio} (see text) at 1000 and 3000 cm^{-1} in FeSe for $p_{bellows} = 1.2$ bar (i.e., $p_{sample} \approx 18.5$ MPa), read from Fig. 2[18]. ΔR^{sat}_{ratio} is normalized by its value at $T_0 = 5$ K. The same quantity at 1500 cm^{-1} for $BaFe_2As_2$[4], normalized at $T_0 = 10$ K, is shown with dashed-double dot line as guide to the eyes. ΔR^{sat}_{ratio} is compared to the T-dependence of the mean-field (MF) order parameter. The stressed-induced orthorhombicity (δ) at typical stress for fully detwinned specimens (i.e., at saturation) is reproduced from Ref. 36 for $BaFe_2As_2$ and estimated for FeSe[37], respectively. The T-axis has been normalized by $T_s \sim$ 90 K and 135 K for FeSe and $BaFe_2As_2$, respectively (vertical dotted line).

optical anisotropy at infrared frequencies, consistent in the $\omega \to 0$ limit with the measured dc one for detwinned samples[19]. As shown in Fig. 3 and elaborated in Ref. 16, ΔR^{sat}_{ratio} remains constant at $T < T_c$, which is compatible with our previous results on Co-doped 122 materials[5]. Even though the impact of superconductivity on the excitation spectrum generally occurs at much lower energy scales, the high energy optical anisotropy, addressed here at $T < T_c$, indicates that the superconducting state develops within a polarized electronic structure. Similarly, the orthorhombic lattice distortion is barely affected by superconductivity in FeSe[19].

Our reflectivity data on FeSe point out the complex evolution of the electronic anisotropy across the structural/nematic phase transition and highlight the important role of the orbital degrees of freedom[11,20–24], affecting the band structure far from the Fermi energy[25]. The optical anisotropy indeed occurs within the frequency interval 0 - 6000 cm^{-1} (Fig. 1), which is fairly consistent with the extent from the Fermi level of the correlated (squeezed) $3d$ iron bands[11,26,27]. However, the detailed nature of the nematic state in FeSe is still debated. A so-called on-site ferro-orbital ordering, even though in agreement with conclusions drawn from NMR investigations[28,29], needs to be reconsidered within momentum dependent scenarios. In fact, ARPES results[10–13,27,30–34] indicate that the electronic band structure in FeSe undergoes a rather intricate momentum-dependent behavior, possibly consistent with either the bond-type ordering of the iron d_{xy}, d_{xz} and d_{yz} orbitals when crossing T_s[12,13,35], the non-trivial energy splitting between the Γ and M point of the Brillouin zone[10], leading to a band shift reversion, or finally the orbital-dependent Fermi-surface shrinking[11]. These scenarios are likely reflected in the optical anisotropy in FeSe and could account for its extension in energy and the change of sign in ΔR_{ratio}, as observed between 1000 and 3000 cm^{-1} (Fig. 1). Moreover, the energy splitting among the d orbitals as evinced from ARPES data[10] follows a mean-field like T-dependence, in agreement with the T-dependence of ΔR^{sat}_{ratio} at both energy scales (Fig. 3). This latter observation underscores the key role of the anisotropic electronic structure with respect to the nematic phase transition.

The hysteretic p-dependence of the optical anisotropy reported here for FeSe is qualitatively reminiscent of what we have observed in $Ba(Fe_{1-x}Co_x)_2As_2$[4,5]. Nonetheless, there are some distinct features, when comparing both materials at equivalent effectively felt uniaxial stress. First of all, the hysteretic behavior of the optical anisotropy in Co-doped $BaFe_2As_2$ is clearly established only at frequencies below 2000 cm^{-1} with $R_a(\omega) > R_b(\omega)$ and without any sign change over the whole spectral range. Moreover the anisotropy at saturation was found to display a broad crossover through the structural transition (Fig. 3), similar to the T-dependence of the dc anisotropy for fully detwinned specimens[2,4,5] and directly comparable to the stress-induced orthorhombicity (Fig. 3)[36]. Even though the dc transport anisotropy in FeSe also exhibits a significant stress-induced tail above T_s[19], ΔR^{sat}_{ratio} at 3000 cm^{-1} displays in contrast a rather sudden drop on approaching T_s from low temperatures, whereas ΔR^{sat}_{ratio} at 1000 cm^{-1} even appears to undergo a sign change on crossing T_s. We conclude that, at least at the energy scales addressed here, the anticipated stress-induced lattice distortion (Fig. 3) above T_s in FeSe[37] may be less strongly or not obviously bound to the electronic structure as in other iron-based superconductors.

As future outlook, it remains to be seen how the anisotropy of the electronic structure in the nematic phase of FeSe, unfolded here, affects energy scales much closer to the Fermi level and thus more pertinent for the anisotropic dc transport[19]. This is of relevance within the debate on the detailed nature of the ordering in FeSe and as to whether scenarios based on anisotropic Fermi surface parameters, favored by our present results, or alternatively substantial spin fluctuations, as envisaged by recent neutron scattering experiments[38,39], trigger the onset of the nematic phase[40–46]. Our ongoing analysis of the far-infrared spectra, in the spirit of Ref. 47 and within the framework of Ref. 48, could serve that purpose.

Acknowledgements

The authors wish to thank C. Mirri for her initial contribution in designing the mechanical pressure device and R. Fernandes, M. Schütt, L. Benfatto, L. Fanfarillo, B. Valenzuela, E. Bascones and M. Watson for fruitful discussions. This work was supported by the Swiss National Foundation for the Scientific Research. Work at the Ames Laboratory was supported by the Department of Energy, Basic Energy Sciences, Division of Materials Sciences and Engineering, under Contract No. DE-AC02-07CH11358. AEB acknowledges support from the Helmholtz Association via PD-226.

* Correspondence and requests for materials should be addressed to: L. Degiorgi, Laboratorium für Festkörperphysik, ETH - Zürich, 8093 Zürich, Switzerland; email: degiorgi@solid.phys.ethz.ch.

[1] A.V. Chubukov, M. Khodas, and R.M. Fernandes, Phys. Rev. X **6**, 041045 (2016) and references therein.

[2] I.R. Fisher, L. Degiorgi, and Z.X. Shen, Rep. Prog. Phys. **74**, 124506 (2011) and references therein.

[3] M.A. Tanatar, A. Kreyssig, S. Nandi, N. Ni, S.L. Bud'ko, P.C. Canfield, A.I. Goldman, and R. Prozorov, Phys. Rev. B **79**, 180508(R) (2009).

[4] C. Mirri, A. Dusza, S. Bastelberger, J.-H. Chu, H.-H. Kuo, I.R. Fisher, and L. Degiorgi, Phys. Rev. B **89**, 060501(R) (2014), and Supplemental Material therein.

[5] C. Mirri , A. Dusza, S. Bastelberger, J.-H. Chu, H.-H. Kuo, I.R. Fisher, and L. Degiorgi, Phys. Rev. B **90**, 155125 (2014).

[6] Any phase transition that breaks a point group symmetry naturally leads to domain formation. In the case of a ferroelastic-like tetragonal-to-orthorhombic transition, as exhibited by underdoped iron-arsenide superconductors as well as by FeSe, a spontaneous strain at low temperatures can be oriented in one of two possible directions, and a twin domain structure forms to minimize the elastic energy[2,3].

[7] J.-H. Chu, H.-H. Kuo, J.G. Analytis, and I.R. Fisher, Science **337**, 710 (2012).

[8] F.C. Hsu, J.-Y. Luo, K.-W. Yeh, T.-K. Chen, T.-W. Huang, P.M. Wu, Y.-C. Lee, Y.-L. Huang, Y.-Y. Chu, D.-C. Yan, and M.-K. Wu, PNAS **105**, 14262 (2008).

[9] T.M. McQueen, A.J. Williams, P.W. Stephens, J. Tao, Y. Zhu, V. Ksenofontov, F. Casper, C. Felser, and R.J. Cava, Phys. Rev. Lett. **103**, 057002 (2009).

[10] Y. Zhang, M. Yi, Z.-K. Liu, W. Li, J.J. Lee, R.G. Moore, M. Hashimoto, M. Nakajima, H. Eisaki, S.-K. Mo, Z. Hussain, T.P. Devereaux, Z.-X. Shen, and D.H. Lu, Phys. Rev. B **94**, 115153 (2016).

[11] L. Fanfarillo, J. Mansart, P. Toulemonde, H. Cercellier, P. Le Fèvre, F. Bertran, B. Valenzuela, L. Benfatto, and V. Brouet, Phys. Rev. B **94**, 155138 (2016).

[12] M.D. Watson, T.K. Kim, L.C. Rhodes, M. Eschrig, M. Hoesch, A.A. Haghighirad, and A.I. Coldea, Phys. Rev. B **94**, 201107(R) (2016).

[13] M.D. Watson, A.A. Haghighirad, L.C. Rhodes, M. Hoesch, and T.K. Kim, cond-mat/1705.02286 (2017).

[14] A.E. Böhmer, V. Taufour, W.E. Straszheim, T. Wolf, and P.C. Canfield, Phys. Rev. B **94**, 024526 (2016).

[15] M. Dressel and G. Grüner, *Electrodynamics of Solids*, Cambridge University Press, Cambridge, England (2002).

[16] See Supplemental Material at [URL will be inserted by publisher] for further details of the samples preparation and experimental technique as well as additional experimental protocols and complementary data.

[17] Each experimental protocol was repeated several times for each combination of T and p. Therefore, ΔR_{ratio} as a function of p, representing the optical anisotropy and shown in Fig. 2, was obtained as average of equivalent experiments. ΔR_{ratio} is evaluated at 1000 and 3000 cm^{-1}, at which frequencies the largest impact of p (i.e., the largest optical anisotropy) is observed.

[18] With respect to the normalized view of ΔR^{sat}_{ratio} in Fig. 3, it is worth reminding that as shown in Fig. 1(b-e) $\Delta R_{ratio} > 0$ and $\Delta R_{ratio} < 0$ at 1000 cm^{-1} and at 3000 cm^{-1}, respectively.

[19] M.A. Tanatar, A.E. Böhmer, E.I. Timmons, M. Schütt, G. Drachuck, V. Taufour, K. Kothapalli, A. Kreyssig, S.L. Budko, P.C. Canfield, R.M. Fernandes, and R. Prozorov, Phys. Rev. Lett. **117**, 127001 (2016).

[20] C.-C. Lee, W.-G. Yin, and W. Ku, Phys. Rev. Lett. **103**, 267001 (2009).

[21] C.-C. Chen, J. Maciejko, A.P. Sorini, B. Moritz, R.R.P. Singh, and T.P. Devereaux, Phys. Rev. B **82**, 100504(R) (2010).

[22] W. Lv, F. Krüger, and P. Phillips, Phys. Rev. B **82**, 045125 (2010).

[23] M. Daghofer, Q.-L. Luo, R. Yu, D.X. Yao, A. Moreo, and E. Dagotto, Phys. Rev. B **81**, 180514(R) (2010).

[24] L. Fanfarillo, G. Giovannetti, M. Capone, and E. Bascones, Phys. Rev. B **95**, 144511 (2017).

[25] L. Benfatto and E. Cappelluti, Phys. Rev. B **83**, 104516 (2011).

[26] M.D. Watson, S. Backes, A.A. Haghighirad, M. Hoesch, T.K. Kim, A.I. Coldea, and R. Valentí, Phys. Rev. B **95**, 081106(R) (2017).

[27] D.V. Evtushinsky, M. Aichhorn, Y. Sassa, Z.-H. Liu, J. Maletz, T. Wolf, A.N. Yaresko, S. Biermann, S.V. Borisenko, and B. Büchner, cond-mat/1612.02313 (2016).

[28] S.-H. Baek, D.V. Efremov, J.M. Ok, J.S. Kim, and J. van den Brink, and B. Büchner, Nature Mat. **14**, 210 (2014).

[29] A.E. Böhmer, T. Arai, F. Hardy, T. Hattori, T. Iye, T. Wolf, H. v. Löhneysen, K. Ishida, and C. Meingast, Phys. Rev. Lett. **114**, 027001 (2015).

[30] A. Fedorov, A. Yaresko, T.K. Kim, Y. Kushnirenko, E. Haubold, T. Wolf, M. Hoesch, A. Grüneis, B. Büchner, and S.V. Borisenko, Scientific Report **6**, 36834 (2016).

[31] P. Zhang, T. Qian, P. Richard, X.P. Wang, H. Miao, B.Q. Lv, B.B. Fu, T. Wolf, C. Meingast, X.X. Wu, Z.Q. Wang, J.P. Hu, and H. Ding, Phys. Rev. B **91**, 214503 (2015).

[32] Y. Suzuki, T. Shimojima, T. Sonobe, A. Nakamura, M. Sakano, H. Tsuji, J. Omachi, K. Yoshioka, M. Kuwata-Gonokami, T. Watashige, R. Kobayashi, S. Kasahara, T. Shibauchi, Y. Matsuda, Y. Yamakawa, H. Kontani, and K. Ishizaka, Phys. Rev. B **92**, 205117 (2015).

[33] Yu.V. Pustovit and A.A. Kordyuk, Low Temp. Phys. **42**, 995 (2016) and references therein.

[34] A.I. Coldea and M.D. Watson, cond-mat/1706.00338 (2017).

[35] K. Jiang, J. Hu, H. Ding, and Z. Wang, Phys. Rev. B **93**, 115138 (2016).

[36] X. Lu, K.-F. Tseng, T. Keller, W. Zhang, D. Hu, Y. Song, H. Man, J.T. Park, H. Luo, S. Li, A.H. Nevidomskyy, and P. Dai, Phys. Rev. B **93**, 134519 (2016).

[37] The stress-induced orthorhombicity in FeSe above T_s can be reasonably estimated for effectively applied stress of about 18 MPa (i.e., at saturation) from the elastic constant and x-ray diffraction data (G.A. Zvyagina, T.N. Gaydamk, K.R. Zhekov, I.V. Bilich, V.D. Fil, D.A. Chareev, and A.N. Vasiliev, Europhys. Lett. **101**, 56005 (2013) and K. Kothapalli, A.E. Böhmer, W.T. Jayasekara, B.G. Ueland, P. Das, A. Sapkota, V. Taufour, Y. Xiao, E. Alp, S.L. Budko, P.C. Canfield, A. Kreyssig, and A.I. Goldman, Nature Commun. **7**, 12728 (2016)). It is comparable to values measured in $BaFe_2As_2$[36].

[38] Q. Wang, Y. Shen, B. Pan, Y. Hao, M. Ma, F. Zhou, P. Steffens, K. Schmalzl, T.R. Forrest, M. Abdel-Hafiez, X. Chen, D.A. Chareev, A.N. Vasiliev, P. Bourges, Y. Sidis, H. Cao, and J. Zhao, Nature Mat. **15**, 159 (2016).

[39] Q. Wang, Y. Shen, B. Pan, X. Zhang, K. Ikeuchi, K. Iida, A.D. Christianson, H.C. Walker, D.T. Adroja, M. Abdel-Hafiez, X. Chen, D.A. Chareev, A.N. Vasiliev, and J. Zhao , Nature Commun. **7**, 12182 (2016).

[40] C. Fang, H. Yao, W.-F. Tsai, J.P. Hu, and S.A. Kivelson, Phys. Rev. B **77**, 224509 (2008).

[41] R.M. Fernandes, A.V. Chubukov, J. Knolle, I. Eremin, and J. Schmalian, Phys. Rev. B **85**, 024534 (2012) and Erratum, Phys. Rev. B **85**, 109901 (2012).

[42] C. Xu, M. Müller, and S. Sachdev, Phys. Rev. B **78**, 020501(R) (2008).

[43] S. Avci, O. Chmaissem, J.M. Allred, S. Rosenkranz, I. Eremin, A.V. Chubukov, D.E. Bugaris, D.-Y. Chung, M.G. Kanatzidis, J.-P. Castellan, J.A. Schlueter, H. Claus, D.D. Khalyavin, P. Manuel, A. Daoud-Aladine, and R. Osborn, Nature Commun. **5**, 3845 (2014).

[44] R.M. Fernandes, A.V. Chubukov, and J. Schmalian, Nature Physics **10**, 97 (2014).

[45] F. Wang, S.A. Kivelson, and D.-H. Lee, Nature Physics **11**, 959 (2015).

[46] A.V. Chubukov, R.M. Fernandes, and J. Schmalian, Phys. Rev. B **91**, 201105 (2015).

[47] C. Mirri, A. Dusza, S. Bastelberger, M. Chinotti, J.-H. Chu, H.-H. Kuo, I.R. Fisher, and L. Degiorgi, Phys. Rev. Lett. **115**, 107001 (2015).

[48] M. Schütt, J. Schmalian, and R.M. Fernandes, Phys. Rev. B **94**, 075111 (2016).